DOI: 10.1002/ejic.200900060

Controlled Synthesis of Terbium Orthophosphate Spindle-Like Hierarchical Nanostructures with Improved Photoluminescence

Jinrong Bao,[a,b] Ranbo Yu,*[a] Jiayun Zhang,[a] Xiaodan Yang,[a] Dan Wang,[c] Jinxia Deng,[a] Jun Chen,[a] and Xianran Xing*[a]

Keywords: Self-assembly / Hydrothermal synthesis / Luminescence / Nanostructures

Nanostructured terbium orthophosphate ($TbPO_4·H_2O$) nanostructures with enhanced photoluminescence were prepared through a controlled, simple, and template-free hydrothermal route. The structures and micromorphologies of the as-synthesized $TbPO_4·H_2O$ were investigated by X-ray powder diffraction (XRD), thermogravimetric analysis, differential scanning calorimetry (TG-DSC), field-emission scanning electronic microscopy (FE-SEM), and X-ray photoelectron spectroscopy (XPS). The results showed that the $TbPO_4·H_2O$ spindle-like hierarchical nanostructures are composed of ordered nanorods of 80–90 nm in diameter and lengths of up to 200–300 nm. It was found that the reactant molar ratios and pH values played key roles in the morphology control of the product. A possible formation mechanism for the spindle-like morphology is also proposed. A photoluminescence study of the products indicated that the self-assembled spindle-like nanostructures display better photoluminescence than $TbPO_4·H_2O$ that was synthesized on both the nano- and microscale.

Introduction

The fabrication of nano- to microscale inorganic structures assembled by nanoparticles, nanorods/nanowires, and nanobelts as building blocks with well-defined shapes and inner structures has attracted great interest as a result of their novel properties and application convenience.[1,2] In particular, much effort has been made to understand the dependency of novel physical and chemical properties of 1D nanostructured materials on the low dimensionality and the quantum confinement effect.[3,4] Moreover, exploring hierarchical self-assembly of 1D nanoscale building blocks into nano-/microstructures might be critical for the development of a nanodevices with high performance.[5–9] Lanthanide orthophosphates ($LnPO_4$), a family of important phosphate compounds, have been studied intensively on the basis of their special physical and chemical properties from their 4f electrons.[10–14] Lanthanide orthophosphates $LnPO_4·nH_2O$ have a variety of potentially beneficial properties, including very low solubility in water (pK_{sol} = 25–27),[15] high thermal stability with melting points up to 2300 °C,[16] high index of refraction, and high concentration of lasing ions.[17] These properties provide the basis for their use in a wide range of applications such as luminescence or laser materials, moisture sensors, heat-resistant materials, and nuclear waste disposal.[18–20]

Very recently, lanthanide compound and lanthanide-doped nanowires with interesting optical properties were successfully prepared by a conventional hydrothermal process.[11,21,22] However, these reported results always show very broad size distributions and nonuniform morphologies. By using the surfactant-assisted process, the $CePO_4$ and $CePO_4$:Tb nanowires with a narrow diameter distribution and uniform morphology could be hydrothermally synthesized,[23] and $LnPO_4$ and $LnPO_4$:Ln^{3+} nanocrystals with a narrow size dispersion and good optical properties were obtained by using a high-boiling-solvent technique.[24,25] Luminescent $LaPO_4$:Ce,Tb nanoparticles with high quantum yields were recently prepared by using a microwave-assisted synthesis method with some ionic liquids as the reaction media.[26] The $TbPO_4·H_2O$ microstructure with mixed spherical and rod-like morphologies was prepared by crystallization from boiling phosphoric acid solution.[27] So far, research about $LnPO_4$ or lanthanide-doped $LnPO_4$ are mainly focused on 1D nanowires/rods or nanoparticles. Therefore, for a given $LnPO_4$, it remains a challenge to establish a suitable reaction system for growing the high quality nano-/microstructured products with controlled-size/shape and manipulated self-assembled ability by a green, facile, and economic strategy.

[a] Department of Physical Chemistry, University of Science and Technology Beijing,
Beijing 100083, China
Fax: +86-10-62332525
E-mail: ranboyu@metall.ustb.edu.cn
xing@ustb.edu.cn
[b] School of Chemistry and Chemical Engineering, University of Inner Mongolia,
Hohhot 010021, China
[c] Key Laboratory of Multi-Phase and Complex System, Institute of Process Engineering, Chinese Academy of Sciences,
Beijing 100190, China

Supporting information for this article is available on the WWW under http://www.eurjic.org or from the author.

Herein, we developed a facile template-free hydrothermal route to synthesize uniform spindle-like nanostructured terbium phosphate hydrate by adjusting the reactant PO_4/Tb molar ratios and pH values. By using this method, the synthesis of $TbPO_4·H_2O$ nanowires and hierarchical, self-assembled, spindle-like nanostructures could be realized, and the latter showed improved photoluminescence. The dependence of the photoluminescent properties on the morphologies of the products was investigated.

Results and Discussion

Synthesis of lanthanide-based phosphate reported in the literature usually starts from the corresponding lanthanide oxide (Ln_2O_3), which is dissolved in concentrated phosphoric acid.[30] A restriction of this route is the limited quantitative dissolution of La_2O_3 in phosphoric acid, which is difficult by control of the temperature and pH, often resulting in nonstoichiometric products. Alternatively, the hydrothermal reaction of $Tb(NO_3)_3·6H_2O$ with highly concentrated phosphoric acid was investigated in this work, and correspondingly, terbium phosphates with high purity and uniform morphologies could be obtained.

The crystal structure and the phase purity of the products were identified by X-ray diffraction analysis (XRD). In Figure 1, we show the typical XRD pattern of the spindle-like nanostructures. All diffraction peaks agree well with a hexagonal structure of $TbPO_4·H_2O$ [space group $P3_121$ (152), PDF card no 20–1244].[22,28] Thermogravimetric analysis (TGA) further confirmed the hydrated nature of the derived hexagonal terbium phosphate (Figure S1, Supporting Information). The endothermic peak at around 193 °C in the differential scanning calorimetry (DSC) curve of the as-synthesized product is consistent with a sudden weight loss of 6.73% in the TG plot, which results from the loss of about 1 mol of H_2O from the product. This clearly indicated that the composition of the product is $TbPO_4·H_2O$. The morphology, as revealed by field-emission scanning electron microscopy (FE-SEM) and transmission electron microscopy (TEM) images (Figure 2a–c), showed that the as-synthesized product consists of spindle-like microparticles with diameters of about 300–400 nm and lengths of about 1 μm, which were self-organized from $TbPO_4·H_2O$ nanorods with diameters of 80–90 nm and lengths of up to 200–300 nm. The surface of these spindle-like particles is not smooth. Notably, almost 100% of the $TbPO_4·H_2O$ nanorods were self-assembled into these spindle-like hierarchical microarchitectures. The electron diffraction pattern recorded on one nanorod indicated that they are single crystals (Figure 2c).

Comparative experiments were carried out to investigate the influence of the reactant PO_4/Tb molar ratios and pH values of the solution on the sizes and morphologies of the products. When the pH values were adjusted from 2.0 to 3.0 by adding ammonia (25%), the as-synthesized $TbPO_4·H_2O$ exhibits a uniform jujube-like morphology (Figure 3a), with an average diameter of about 500–600 nm. Subsequently,

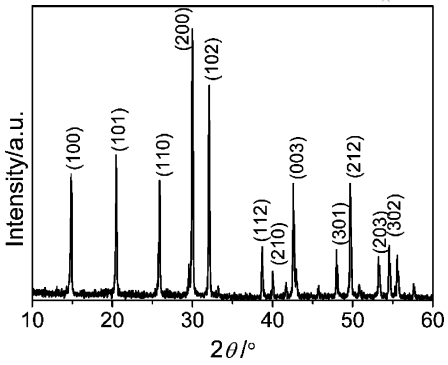

Figure 1. XRD pattern of the $TbPO_4·H_2O$ spindle–like nanostructures.

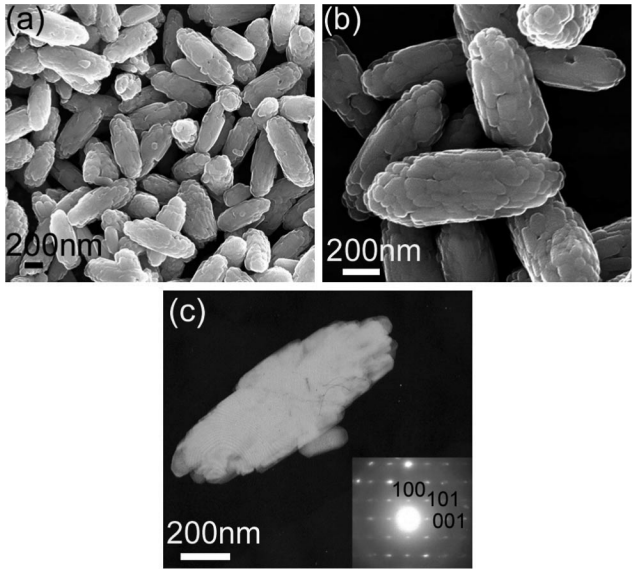

Figure 2. FE-SEM images of $TbPO_4·H_2O$ spindle-like nanostructures: (a) low-magnification image, (b) high-magnification image, (c) TEM image and selected area electron diffraction image.

the pH values were increased from 4.0 to 6.0 and the morphology of the products changed into uniform sphere-like microstructures (Figure 3b). The reactant PO_4/Tb molar ratio is one of the most important factors in our experiment. When the reactant PO_4/Tb molar ratios are 40 to 60, without ammonia (25%), uniform hexagonal prisms were obtained (Figure 3c), which are about 700–800 nm in diameter. Furthermore, when the reactant PO_4/Tb molar ratio is 10, the product $TbPO_4·H_2O$ is composed of nanowires with diameters of 80–90 nm and lengths of about 1 μm (Figure 3d). The X-ray diffraction patterns (Figure S2, Supporting Information) of the different morphologies can be indexed to the hexagonal structure $TbPO_4·H_2O$ [space group $P3_121$ (152), PDF card no 20–1244].

Therefore, the morphologies of the products can be controlled well by tuning the reactant PO_4/Tb molar ratios and solution pH values without the presence of any other organic additives. Generally, $LnPO_4$ tends to grow as 1D nanowires, which is possibly due to the 1D characteristics

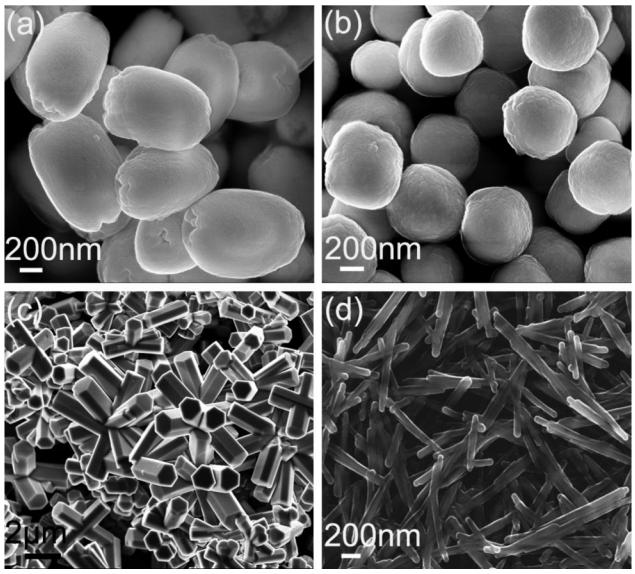

Figure 3. FE-SEM images of the products corresponding to different morphologies: (a) jujube-like, (b) sphere-like, (c) hexagonal prisms, (d) nanowires.

of the infinite linear chains of hexagonal-structured $LnPO_4$ (Ln = La–Dy).[21] When the PO_4/Tb molar ratio is lower than 10, the $TbPO_4·H_2O$ product grow as 1D nanowires, whereas when the PO_4/Tb molar ratio is higher than 40, $TbPO_4·H_2O$ with a small length-to-diameter ratio could be obtained. The $TbPO_4·H_2O$ hexagonal prisms were grown and crystallized with a starting PO_4/Tb molar ratio of 40. Furthermore, the spindle-like, jujube-like, and sphere-like morphologies with uniform sizes could be obtained with highly concentrated acid by increasing the pH values. Apparently, the growth tendency of $TbPO_4·H_2O$ as 1D nanowires could be restrained at high concentrations of phosphoric acid.

To understand the growth mechanism of the spindle-like $TbPO_4·H_2O$ nanostructures, the growth process was studied by time-dependent XRD patterns. The XRD patterns of the products obtained after hydrothermal treatment for 0, 2, and 8 h are given in Figure S3 (Supporting Information). The $NH_4H_2PO_4$ precipitations could be detected in the products after hydrothermal treatment for 0 and 2 h. When the reaction time was prolonged to 8 h, pure $TbPO_4·H_2O$ could be obtained. If the pH value was adjusted to 6.0, a longer hydrothermal treatment time of 24 h was necessary for the formation of pure $TbPO_4·H_2O$. Therefore, the proposed mechanism for the hydrothermal synthesis of $TbPO_4·H_2O$ by adjusting the pH value with the use of ammonia might be as follows:

$$NH_3·H_2O + H_3PO_4 \leftrightarrow NH_4H_2PO_4 + H_2O$$

$$NH_4H_2PO_4 + Tb^{3+} + H_2O \leftrightarrow TbPO_4·H_2O + NH_4^+ + 2H^+$$

Because the spindle-like $TbPO_4·H_2O$ nanostructures were obtained with reactant PO_4/Tb molar ratios from 40 to 60, a terbium phosphate nucleus could be formed rapidly with the use of concentrated phosphoric acid. However, with highly concentrated acid, the as-obtained terbium phosphate nucleus would soon dissolve. With the addition of ammonia (25%) to this system, $NH_4H_2PO_4$ would be easily formed, which could then react with Tb^{3+} to form $TbPO_4·H_2O$. The formation of $NH_4H_2PO_4$ could decrease the rapid growth and crystallization of $TbPO_4·H_2O$ and might be helpful to control the growth and aggregation of the $TbPO_4·H_2O$ nanorods. In our case, phosphoric acid is very much in excess, and the electrostatic potential on the crystal surface of initially formed $TbPO_4·H_2O$ particles will increase, which results in high surface energy. To minimize the surface energy[29] these nanorods assemble and crystallize into spindle-like nanostructures as the reaction time increases.

The probable growth process of $TbPO_4·H_2O$ crystals with spindle-like nanostructures is illustrated in Figure 4. In our current reaction system, the reactant PO_4/Tb molar ratio was changed from 40 to 60. When using ammonia (25%) to adjust the pH value, $NH_4H_2PO_4$ precipitation will be formed at an early stage of the reaction, which could affect the rapid formation of $TbPO_4·H_2O$ nanorods. The excess H_3PO_4 might be responsible for the electrostatic potential increase on the crystal surfaces of initially formed $TbPO_4$ particles. To minimize the surface energy these nanorods might assemble and crystallize into spindle-like nanostructures as the reaction time increases.

Room-temperature photoluminescence (PL) spectra were recorded for solid products of different morphologies (Figure 5). When these species were excited at 222 nm, emission peaks centered at 488, 542, 585, and 618 nm were observed, which could contribute to the $^5D_4 \rightarrow {}^7F_6$, $^5D_4 \rightarrow {}^7F_5$, $^5D_4 \rightarrow {}^7F_4$, and $^5D_4 \rightarrow {}^7F_3$ transitions, respectively.[24] Although the major peaks in the emission spectra are identical in these products, the intensity patterns are different. Additionally, it was observed that the relative intensity ratios

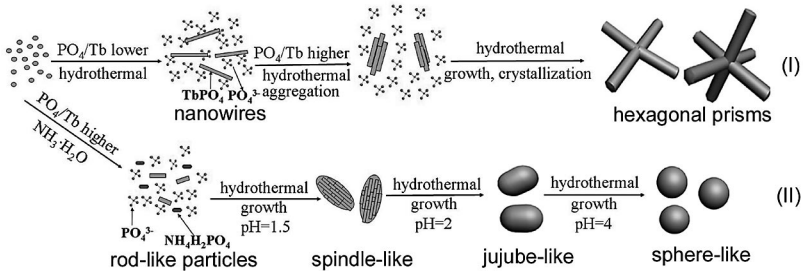

Figure 4. Schematic illustration showing the mechanism of formation of the $TbPO_4·H_2O$ spindle-like nanostructures.

of the $^5D_4 \rightarrow {}^7F_5$ and $^5D_4 \rightarrow {}^7F_6$ transitions in the hexagonal prisms are different from the other four morphologies, and the calculated relative intensity ratio of the hexagonal prisms is larger than that of the other morphologies. These results indicate that the PL properties can be affected by various dimensions, morphologies, and sizes. Interestingly, the spindle-like nanostructures with self-assembly of the ordered nanorods showed the strongest photoluminescence, which might resulted from the less diminished hydroxy quenching at the surfaces of the spindle-like nanostructures. To further confirm the hydroxy-quenching effect of the products, X-ray photoelectron spectroscopy (XPS) analysis was performed (Figure S4, Supporting Information). The XPS peaks corresponding to O1s for $TbPO_4 \cdot H_2O$ with different morphologies are shown in Figure S4a (Supporting Information). In the case of the O1s peaks, a shoulder at 533 eV is observed with the main peak at 531 eV. The main peak is assigned to the lattice oxygen, and the shoulder is due to the oxygen of the metal-OH bonds.[30] Figure S4b (Supporting Information) shows the O1s peaks, which were fitted with two Gaussian functions. As a result of the difficulty in defining each hydroxide, the width or position of the fitted peaks are not fixed. Figure S4c (Supporting Information) shows the change in the OH^-/O^{2-} integrated-intensity ratios with morphology evolution. As the morphologies of products evolved from spindle-like nanostructures, nanowires, and spheres, the OH^-/O^{2-} integrated-intensity ratios increased. Correspondingly, the PL intensities of these three samples decreased. Moreover, the spindle-like nanostructures even showed stronger PL than the as-synthesized microscaled hexagonal prisms. These revealed that the self-assembly of the nanorod building blocks into nano-/microstructures is of great significance to enhance the PL properties. Further research about the relations between the PL properties and the morphologies is in progress.

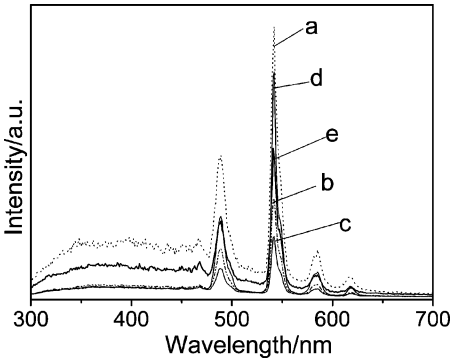

Figure 5. Photoluminescence spectra of the products with different morphologies: (a) spindle-like, (b) jujube-like, (c) sphere-like, (d) hexagonal prisms, (e) nanowires.

Conclusions

In summary, nanostructured $TbPO_4 \cdot H_2O$ with enhanced photoluminescent properties were prepared through a controlled synthesis by using a simple, template-free, hydrothermal route, and nano-/microsized $TbPO_4 \cdot H_2O$ structures with a diverse range of well-defined morphologies were successfully synthesized. The relationship between the morphologies and the reaction conditions were systematically investigated. It was found that the morphologies of $TbPO_4 \cdot H_2O$ can be controlled by adjusting PO_4/Tb molar ratios and the solution pH values. The growth mechanism study indicated that the formation of $NH_4H_2PO_4$ played an important role in the formation of nanorods and their self-assembly into uniform, spindle-like, hierarchical nanostructures. Inspiringly, the self-assembly of nanorods could enhance the PL emission. This facile hydrothermal approach may provide a feasible approach for manipulating various uniform nano-/microstructures and building complex architectures with interesting morphologies and optical properties. Further clarification of the dependence of the PL properties on the morphologies will be of significance for developing excellent photoluminescent materials with well-controlled morphologies.

Experimental Section

General: All chemicals were of analytical grade and used as received without further purification. H_3PO_4 (A.R.), HNO_3 (A.R.), NH_3H_2O (A.R.), and Tb_2O_3 (purity > 99.99%) were all supplied by Beijing Chemical Reagent Company. $Tb(NO_3)_3 \cdot 6H_2O$ powder prepared from Tb_2O_3 was dissolved in 10% nitric acid and then evaporated and dried in vacuo. Characterization of the X-ray powder diffraction (XRD) patterns of all samples were recorded with a 21 kW extra-power X-ray diffractometer (Model M21XVHF22, MAC Science Co., Ltd., Japan) by using Cu-K_α radiation (λ = 0.1541 nm) in the range 10–60° at room temperature. Thermogravimetric analysis (TGA) coupled with differential scanning calorimetry (DSC) was performed up to 600 °C at a heating rate of 10 °C min^{-1} under air gas flow (Model NETZSCH STA 409 C/CD). The size and morphology of the products were characterized by field-emission scanning electron microscopy (FE-SEM, LEO1530). Transmission electron microscopy (TEM) images and selected area electron diffraction (SAED) patterns were recorded with a JEOL JEM-100CX microscope with an accelerating voltage of 100 kV. The photoluminescence spectra of powders were recorded with an F-4500 FL spectrophotometer at room temperature. The chemical-bond states were analyzed by X-ray photoelectron spectroscopy (XPS, ESCALAB250) with Al-K_α radiation. The binding energy (BE) for the samples was calibrated by setting the measured BE of C1s to 284.6 eV.

Typical Procedure for the Synthesis of $TbPO_4 \cdot H_2O$ Spindle-Like Nanostructures: The appropriate amount of a terbium nitrate solution was added slowly to phosphoric acid (6 M, 10 mL) whilst stirring, and the PO_4/Tb molar ratios were from 40 to 60. Then, the pH value of the as-obtained transparent solution was adjusted to 1.5 with ammonia (25%), and the mixture was transferred into a stainless steel autoclave with an inner Teflon vessel (volume, 50 mL). The autoclave was sealed and maintained at 110 °C for 8 h and then allowed to naturally cool to room temperature. The resulting white solid precipitate was filtered, washed three times with deionized water and absolute alcohol, and finally dried at 60 °C for 8 h.

Supporting Information (see footnote on the first page of this article): XRD patterns, TGA analysis, XPS analysis, and FE-SEM images.

Acknowledgments

The authors are thankful for financial support from the National Natural Science Foundation of China (No. 20871015, 20401015), "Program for New Century Excellent Talents in University" (NCET), and Beijing Natural Science Foundation (No. 2092019).

[1] Y. Y. Xu, D. R. Chen, X. L. Jiao, *J. Phys. Chem. B* **2005**, *109*, 13561–13566.
[2] S. H. Chen, Z. Y. Fan, D. L. Carroll, *J. Phys. Chem. B* **2002**, *106*, 10777–10781.
[3] K. Hiruma, M. Yazawa, T. Katsuyama, K. Ogawa, K. Haraguchi, M. Koguchi, H. Kakibayashi, *J. Appl. Phys.* **1995**, *77*, 447–462.
[4] J. D. Holmes, K. P. Johnston, R. C. Doty, B. A. Korgel, *Science* **2000**, *287*, 1471–1473.
[5] L. Manna, D. J. Milliron, A. Meisel, E. C. Scher, A. P. Alivisatos, *Nat. Mater.* **2003**, *2*, 382–385.
[6] B. Liu, H. C. Zeng, *J. Am. Chem. Soc.* **2004**, *126*, 8124–8125.
[7] X. Feng, J. Zhai, L. Jiang, *Angew. Chem. Int. Ed.* **2005**, *44*, 5115–5118.
[8] H. Shi, X. Wang, N. Zhao, L. Qi, J. Ma, *J. Phys. Chem. B* **2006**, *110*, 748–753.
[9] B. X. Li, G. X. Rong, Y. Xie, L. F. Huang, C. Q. Feng, *Inorg. Chem.* **2006**, *45*, 6404–6410.
[10] G. Y. Adachi, N. Imanaka, *Chem. Rev.* **1998**, *98*, 1479–1514.
[11] R. X. Yan, X. M. Sun, X. Wang, Q. Peng, Y. D. Li, *Chem. Eur. J.* **2005**, *11*, 2183–2195.
[12] S. P. Fricker, *Chem. Soc. Rev.* **2006**, *35*, 524–533.
[13] J. Dhanaraj, R. Jagannathan, T. R. N. Kutty, C.-H. Lu, *J. Phys. Chem. B* **2001**, *105*, 11098–11105.
[14] H. Mass, A. Currao, G. Calzaferri, *Angew. Chem. Int. Ed.* **2002**, *41*, 2495–2497.
[15] F. H. Firsching, S. N. Brune, *J. Chem. Eng. Data* **1991**, *36*, 93–95.
[16] A. Rouanet, J. J. Serra, K. Allaf, V. P. Orlovskii, *Neorg. Mater.* **1981**, *17*, 104–109.
[17] Y. Guo, P. Woznicki, A. Barkatt, E. E. Saad, I. G. Talmy, *J. Mater. Res.* **1996**, *11*, 639–649.
[18] O. Lehmann, K. Kompe, M. Haase, *J. Am. Chem. Soc.* **2004**, *126*, 14935–14942.
[19] K. Riwotzki, H. Meyssamy, A. Kornowski, M. Haase, *J. Phys. Chem. B* **2000**, *104*, 2824–2828.
[20] P. Schuetz, F. Caruso, *Chem. Mater.* **2002**, *14*, 4509–4516.
[21] Y. P. Fang, A. W. Xu, R. Q. Song, H. X. Zhang, L. P. You, J. C. Yu, H. Q. Liu, *J. Am. Chem. Soc.* **2003**, *125*, 16025–16034.
[22] Y. W. Zhang, Z. G. Yan, L. P. You, R. Si, C. H. Yan, *Eur. J. Inorg. Chem.* **2003**, 4099–4104.
[23] W. B. Bu, Z. L. Hua, H. R. Chen, J. L. Shi, *J. Phys. Chem. B* **2005**, *109*, 14461–14464.
[24] K. Riwotzki, H. Meyssamy, H. Schnablegger, A. Kornowski, M. Haase, *Angew. Chem. Int. Ed.* **2001**, *40*, 573–576.
[25] K. Kompe, H. Borchert, J. Storz, A. Lobo, S. Adam, T. Moller, M. Haase, *Angew. Chem. Int. Ed.* **2003**, *42*, 5513–5516.
[26] G. Buhler, C. Feldmann, *Angew. Chem. Int. Ed.* **2006**, *45*, 4864–4867.
[27] R. Kijkowska, *J. Mater. Science.* **2003**, *38*, 229–233.
[28] W. H. Di, X. J. Wang, P. P. Zhu, B. J. Chen, *J. Solid State Chem.* **2007**, *180*, 467–473.
[29] R. L. Penn, J. F. Banfield, *Science* **1998**, *281*, 969–971.
[30] N. S. Ramgir, I. S. Mulla, K. P. Vijayamohanan, *J. Phys. Chem. B* **2005**, *109*, 12297–12303.

Received: January 16, 2009
Published Online: April 27, 2009

